ELSEVIER

Nuclear Instruments and Methods in Physics Research B 171 (2000) 360–372

NIM B
Beam Interactions with Materials & Atoms

www.elsevier.nl/locate/nimb

A model for the operation of helium-filled proportional counter at low temperatures near 4.2 K

Sei Masaoka [a], Rintaro Katano [a], Shunji Kishimoto [b], Yasuhito Isozumi [c,*]

[a] *Institute for Chemical Research, Kyoto University, Uji, Kyoto 611-0011, Japan*
[b] *Photon Factory, Institute of Materials Structure Science, 1-1 Oho, Tsukuba 305-0801, Japan*
[c] *Radioisotope Research Center, Kyoto University, Kyoto 606-8501, Japan*

Received 17 September 1999; received in revised form 4 February 2000

Abstract

In order to understand the operation of helium-filled proportional counter (HFPC) from the standpoint of fundamental atomic and molecular processes, we have surveyed previous works on collision processes in discharged helium gas. By analyzing gas gain curve, after-pulses and discharge current experimentally observed at 4.2 K, the electron avalanche and the secondary electron emission from cathode have been related to the collision processes in helium. A simplified model for the HFPC operation at low temperatures near 4.2 K has been constructed with the related processes. © 2000 Elsevier Science B.V. All rights reserved.

Keywords: CEMS; Low-temperature radiation detector; Helium-filled proportional counter; Liquid helium

1. Introduction

In spite of containing no quenching admixture such as organic gases of CH_4 and C_4H_{10}, a counter filled with helium gas operates in the proportional region at low temperatures near 4.2 K [1–3]. The helium-filled proportional counter (HFPC) is intensively used to detect electrons backscattered from a sample in the cryogenic resonance Mössbauer spectroscopy (REMS) [4–6]; the sample is mounted as a cathode in the counter, the whole of which is cooled at the low temperatures.

Unfavorable behaviors in the HFPC operation at the low temperatures were found by our previous studies [1–3,7–9]. Firstly, the operation is practically limited by the self-sustained electric discharge, which is induced at rather low gas gains (at most 200) [1]. Secondly, the secondary electron emission from cathode injures the HFPC operation even in the proportional region, as revealed by the analysis for the after-pulse [8] and the discharge current [9].

Helium is the simplest atom in noble gas atoms. Many workers have so far investigated various

* Corresponding author. Tel.: +81-75-753-7512; fax: +81-75-753-7504.
E-mail address: yasuhito@barium.rirc.kyoto-u.ac.jp (Y. Isozumi).

0168-583X/00/$ - see front matter
PII: S0168-583X(00)00291-3

collision processes in discharged helium both experimentally and theoretically. With such data, it may be possible to understand the mechanism for the low-temperature HFPC operation from the standpoint of fundamental atomic and molecular processes in helium gas. In this paper, our experimental observations of gas gain, after-pulse and discharge current of the HFPC have been attributed to some fundamental processes in discharged helium. A model for the HFPC operation has been constructed with some parameters determined by reaction rates or transition probabilities of the attributed processes. The model is useful to discuss qualitatively electron avalanche, electron emission from cathode and electric discharge, but it is still difficult to use the model for quantitative discussions because of the lack of reliable data on the rates and the probabilities.

The present HFPC and the experimental apparatus to operate it are briefly described in Section 2. The electron avalanche on anode wire and the electron emission from cathode in the HFPC are related to collision processes in helium gas in Sections 3 and 4, respectively. Some experimental observations to examine the avalanche and the electron emission are also discussed. A model for the HFPC operation is proposed in Section 5. Some discussions on the model and future works are given in Section 6.

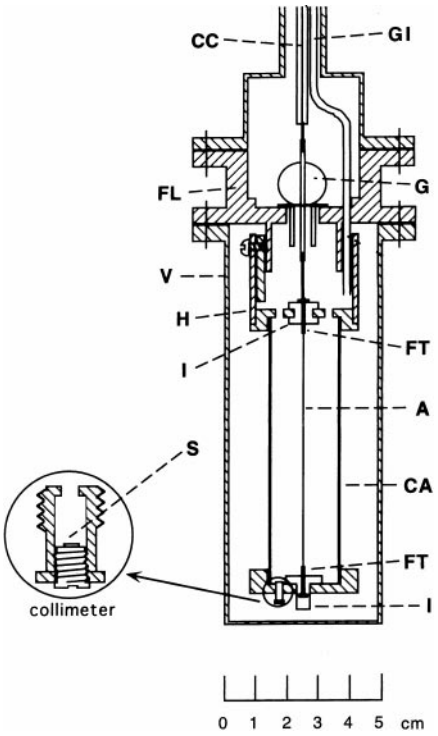

Fig. 1. Layout of the helium-filled proportional counter and the collimator for ^{210}Po source: A: anode (30-μm diameter gold-plated tungsten wire); CA: cathode (25-mm diameter × 76-mm long stainless steel pipe); S: ^{210}Po source; FT: field tube; G: glass feedthrough; I: Teflon insulator; H: aluminum holder; V: stainless steel vessel; GI: gas inlet (3-mm diameter stainless steel pipe); FL: brass flange; CC: coaxial cable.

2. Experiment apparatus

The present apparatus to examine the operation of HFPC is same as used in the previous work [9]. Fig. 1 is a layout of the HFPC; the anode (A) is a 30-μm diameter gold-plated tungsten wire and the cathode (CA) is a 25-mm diameter × 76-mm long stainless steel pipe. The cryostat to cool the HFPC down to 4.2 K is shown in Fig. 2; the HFPC is mounted at the bottom of the cryostat. The length of the signal cable (CC) from the HFPC to the preamplifier outside is about 1 m, of which capacitance is about 50 pF. The preamplifier used is a commercially available one, CANBERRA 2003T, of which the nominal noise (FWHM, Si) is 2.0 keV with no capacitance and the decay time constant is 250 μs. The output from the preamplifier was registered in the digital oscilloscope (Tektronix TDS-220) to observe after-pulse and electric discharge in the HFPC.

Impurities in helium gas, i.e., mainly water, were carefully adsorbed by molecular sieves cooled at liquid nitrogen temperature. Through a 3-mm diameter stainless steal pipe (GI in Figs. 1 and 2), the purified helium was introduced in HFPC at the normal condition, i.e., 760 Torr at room temperature (300 K). After sealing a small valve at the top of the pipe GI, the HFPC was cooled down exactly to 4.2 K by filling the tank (HT in Fig. 2) with liquid helium. The number density of helium gas in the HFPC is 2.45×10^{19} cm^{-3} and the pressure at 4.2 K is 10.4 Torr in the present work.

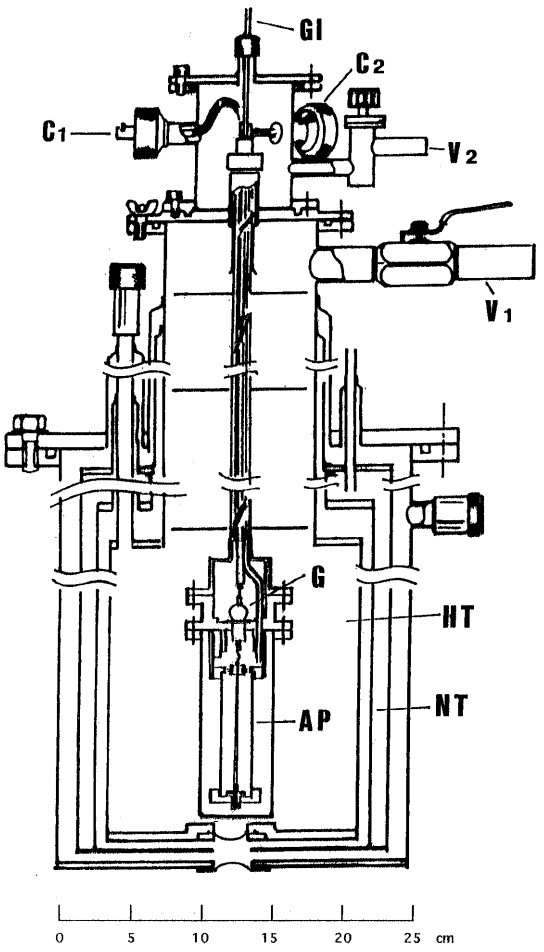

Fig. 2. Layout of the cryostat to mount the helium-filled proportional counter: GI: gas inlet; C1: connector assembly to pick up radiation signals; C2: connecter assembly for thermocouple and others; V1: valve for helium pumping; V2: vacuum valve; HT: liquid helium tank; NT: liquid nitrogen tank; G: glass feedthrough; AP: helium-filled proportional counter.

A ^{210}Po source (S in Fig. 1) was installed at the end plate of the counter; the incident direction of α particles from ^{210}Po is parallel to the anode after passing through a 1-mm diameter hole of collimator. The energy of the α particle from ^{210}Po is 5.3 MeV and its range is 20.8 cm at the normal condition of helium gas. The energy loss of the α particles in the present HFPC with 60-mm sensitive length is estimated to be about 1.5 MeV.

3. Electron avalanche

3.1. Ionization processes in pure helium

In the HFPC, nuclear radiations ionize helium gas to produce pairs of electron and positive ion, of which the number is proportional to the radiation energy deposited in the gas. Electrons produced are attracted to anode, where they successively ionize helium atoms after being accelerated by the steep electric field near anode. Each electron produced in the primary ionization finally grows up to an avalanche, of which the average electron number is defined as *gas gain*.

Two kinds of ionization processes take place in the electron avalanches in pure helium gas. One is the direct ionization caused by the collision of electrons with helium gas atoms, He(1^1S), which also produces a lot of excited heliums, He*. The other process is caused by the collision of the highly-excited helium He* ($n \geqslant 3$) with He(1^1S),

$$\mathrm{He}^* \ (n \geqslant 3) + \mathrm{He} \rightarrow \mathrm{He}_2^+ + \mathrm{e}. \qquad (1)$$

In the above expression, n is the principal quantum number; the energy conservation law inhibits the process (1) for $n = 1$ and $n = 2$ states. This collisional ionization is so called the Hornbeck–Molnar process [10]. The cross-sections of this process for $n = 3$ states are listed in Table 1 [11]. With the cross-sections, the reaction rate of this process is estimated to be nearly $10^7 p$ s^{-1}, where p is the pressure of helium gas in Torr at room temperature.

The excited helium He* ($n \geqslant 3$) de-excites through collisions with helium gas or radiative transition. The cross-sections of collisional relaxations for $n = 3$ states are also listed in Table 1 [12]. As seen in this table, the reaction rate for the de-excitations of $3^3\mathrm{P} \rightarrow 3^3\mathrm{S}$, $3^1\mathrm{P} \rightarrow 3^1\mathrm{S}$, $3^3\mathrm{D} \rightarrow 3^3\mathrm{P}$ and $3^1\mathrm{D} \rightarrow 3^1\mathrm{P}$ is almost the same order as that of the Hornbeck–Molnar process. The probability of the radiative transition is smaller than 10^8 s^{-1}, as discussed in Section 4. This value is at least two orders in magnitude smaller than the reaction rates of the collisional ionization and de-excitations at the normal condition of helium gas, i.e., with a pressure of 760 Torr at room temperature.

Table 1
Cross-sections of Hornbeck–Molnar and collisional relaxation processes

Hornbeck–Molnar process[a]		Collisional relaxation[b]	
State of excited helium	Cross-section (10^{-16} cm^2)	Transition	Cross-section (10^{-16} cm^2)
3^3P	1.6 ± 0.1	$3^3P \rightarrow 3^3S$	2.9 ± 0.3
		$3^3P \rightarrow 3^3D$	0.067 ± 0.005
3^1P	3.1 ± 1.0	$3^1P \rightarrow 3^1S$	4.5 ± 0.03
		$3^3P \rightarrow 3^3D$	32 ± 1
3^3D	4.5 ± 0.5	$3^3D \rightarrow 3^3S$	<0.01
		$3^3D \rightarrow 3^3P$	0.62 ± 0.05
3^1D	20 ± 4	$3^1D \rightarrow 3^1S$	<0.04
		$3^1D \rightarrow 3^1P$	10.6 ± 0.7

[a] Wellenstein and Robertson [11].
[b] Wellenstein and Robertson [12].

The relative population of excitations and ionization of helium atom by electron impact are listed in Table 2, which was estimated for the electron energy of 1230 eV by Alkahzov and Vorob'ev [13]. According to their estimation, the population of ionization is 40.5% while that of excitation is 42.5% for $n = 2$, 9.1% for $n = 3$ and 8.4% for $n \geqslant 4$. The population to $n \geqslant 3$ states becomes 17.5%. As explained above, roughly half of $n \geqslant 3$ states arise the Hornbeck–Molnar process and the other half arise the collisional de-excitation. This means that very roughly 20% ($= 17.5/2/40.5$) of ionization events in the avalanche are caused by the Hornbeck–Molnar process at room temperature.

Table 2
Relative population of excitation and ionization

State	Energy of state (eV)	Relative population[a] (%)
2^3S	19.81	7.6
2^1S	20.61	4.3
2^3P	20.96	3.8
2^1P	21.22	26.8
3^3S	22.72	0.7
3^1S	22.92	0.8
3^3P	23.00	0.6
3^1P	23.08	6.3
3^3D	23.07	0.2
3^1D	23.07	0.5
$n \geqslant 4$	–	8.4
He^+	24.59	40.5

[a] Alkhazov and Vorob'ev [13].

3.2. Estimated and experimental gas gain

The gas gain of a proportional counter can be estimated from the first Townsend ionization coefficient, α (cm^{-1}), which is defined by the number of ionizing events induced by an electron per unit length in the direction of the electric field. The coefficient α is usually measured as a function of X/p [14], where X is the field strength (V cm^{-1}) and p is the pressure of filling gas (Torr). For a cylindrical counter, X is given by

$$X = V_a/[r \ln(b/a)], \tag{2}$$

where V_a is the anode voltage (V), r the distance (cm) from the centerline of the counter in the direction of electric field, a the radius of anode (cm) and b is the radius of cathode (cm). By integrating α over the region of $a \leqslant r \leqslant b$ [7], $G(V_a)$ is expressed as

$$G(V_a) = \exp\left[\int_a^b \alpha\ (t = X/p)\ \mathrm{d}r\right] = \exp\left[U_p \int_{U_p/b}^{U_p/a} \alpha(t)/t^2\ \mathrm{d}t\right], \tag{3}$$

where U_p is given by

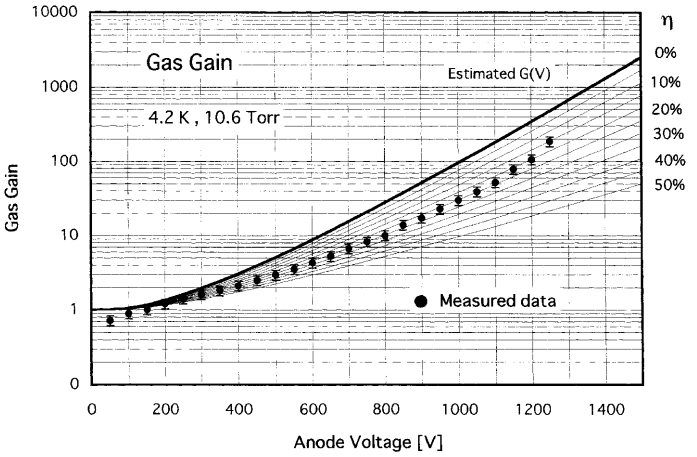

Fig. 3. Gas gain curves $G(V_a)$ as a function of anode voltage, V_a: closed circle, data obtained with the present HFPC; solid curve, estimation from the first Townsend ionization coefficient α experimentally measured; other curves, estimations with various η values (0–50%). The electric discharge takes place at a voltage a little higher than 1250 V and the gas gain at this voltage is about 200. The measured $G(V_a)$ is lower than unity in the region of $V_a < 150$ V because of the recombination between helium ions and electrons.

$$U_p = V_a/[p\ln(b/a)]. \quad (4)$$

According to Eq. (3), the gas gain $G(V_a)$ has been estimated with the coefficient α $(t = X/p)$ measured by Chanin and Rork [15], which was obtained with carefully purified helium at room temperature; results are shown by the bold curve in Fig. 3.

Using the apparatus described in Section 2, $G(V_a)$ has been measured for the condition of helium gas with a pressure of 10.4 Torr at 4.2 K; results are shown by closed circles in Fig. 3. The measured $G(V_a)$ is lower than the estimated one in the whole V_a region. Since the α values by Chanin and Rork [15] were obtained at room temperature, their data contain the contribution from the direct ionization by electrons and that from the Hornbeck–Molnar process. The direct ionization does not depend on the temperature of helium gas because of the relatively high energy of electrons in avalanches. On the other hand, the atom–atom and atom–molecule collisions, such as the Hornbeck–Molnar process, generally depend on the gas temperature, as discussed below. Therefore, the difference between estimated and experimental $G(V_a)$ curves indicates that the ionization by Hornbeck–Molnar process is remarkably suppressed at the low temperature, i.e., 4.2 K. [1]

3.3. Suppression of collision processes at low temperatures

The reaction rate per unit volume of two-body collisions such as the Hornbeck–Molnar process is expressed by

$$v(T) = N(\mathrm{He})N(\mathrm{He}^*)\int_0^\infty v(E)\sigma(E)f_g(E,T)\,\mathrm{d}E = 2N(\mathrm{He})N(\mathrm{He}^*)\sigma_{av}(T)[kT/M]^{1/2}, \quad (5)$$

where $N(\mathrm{He})$ and $N(\mathrm{He}^*)$ are the number densities of He and He^*, respectively, $\sigma(E)$ the cross-section of the two-body collision as a function of collision energy E, v the relative velocity between He and He^*, $f_g(E,T)$ the Maxwell distribution at the gas temperature T, k the Boltzmann constant and M is the mass of the helium atom. The quantity $\sigma_{av}(T)$

[1] In [7], we discussed the other possibility to explain the difference between experimental and estimated $G(V_a)$, i.e., effect of impurities in helium gas in the measurement by Chanin and Rork. This possibility has been denied by the present analysis for $G(V_a)$.

in Eq. (5) is an average of $\sigma(E)$ on the energy E in the Maxwell distribution. When $\sigma_{av}(T)$ has a structure with a steep change like bump or valley, the collision process becomes very sensitive to the gas temperature. The term $T^{1/2}$ in Eq. (5) is also responsible for the sensitivity, indicating that the reaction rate of the two-body collision at 4.2 K is suppressed to 0.12 ($=[4.2/300]^{1/2}$) of the rate at room temperature. In the present situation, it is not possible to make clear which is a main origin for the suppression at the low temperature, the term $T^{1/2}$ or $\sigma_{av}(T)$ in Eq. (5); the Hornbeck–Molnar process has not so far been investigated at low temperatures near 4.2 K.

In Fig. 3, several $G(V_a)$ curves corrected for the suppression at 4.2 K are shown; they are estimated with the α values reduced by a factor η from the values by Chanin and Rork [15], where η is from 0% to 50%. The measured $G(V_a)$ is in the region between the estimated curve for $\eta = 15\%$ and that for $\eta = 35\%$. This is consistent with the contribution of the Hornbeck–Molnar process to the ionization in helium, which is about 20% of that by electron impact at room temperature, as discussed in Section 3. The measured $G(V_a)$ for lower V_a fits to an estimated curve for a larger η value. The contribution of the process is higher for lower V_a at room temperature, because the excitation of helium by electron impact becomes more popular with decreasing electron energy.

4. Electron emission from cathode

4.1. Active particles and electric discharge

Various atomic and molecular processes in the electron avalanche create a lot of active particles such as positive ion, ultra-violet photon and metastable, which can cause additional ionizations through the collision with cathode material in the HFPC. An electron emitted from cathode travels to anode and there induces a new avalanche. Consequently, the electron avalanche initiated by the primary ionization is spread both in space and time by the additional ionizations, resulting in unstable operation or inducing self-sustained electric discharge.

The number of the electrons from cathode per an avalanche, R, is given by a sum of the number of electrons emitted by the collision of positive ions at cathode, R_i, that by the collision of ultra-violet photons, R_p and that by the collision of metastables, R_m [14],

$$R = R_i + R_p + R_m. \tag{6}$$

The parameter R_i is given by

$$R_i = G\Gamma_i, \tag{7}$$

where G is the gas gain and Γ_i is the second Townsend ionization coefficient of the positive ion, i.e., a probability with which an ion emits an electron through the collision with cathode.

Since ultra-violet photons may come from several origins, as discussed below, R_p in Eq. (6) is given as a sum of components $R_{p(k)}$,

$$R_p = \sum_k R_{p(k)}, \tag{8}$$

where each component $R_{p(k)}$ is expressed as

$$R_{p(k)} = GP_{p(k)}\varepsilon_{p(k)}\Gamma_{p(k)}. \tag{9}$$

In the above expression, $P_{p(k)}$ is the relative population (per ionization events in an avalanche) of helium excited atoms or molecules which emit ultra-violet photons as the kth origin, $\varepsilon_{p(k)}$ is a ratio of the reaction rate of the photon production to that of all decaying processes for the excited atom and molecules and $\Gamma_{p(k)}$ is the second Townsend ionization coefficient for the kth photon.

The parameter R_m for metastables is given by

$$R_m = GP_m\varepsilon_m\Gamma_m, \tag{10}$$

where P_m, ε_m and Γ_m are similarly defined as those for ultra-violet photons. Note that $P_{p(k)}\varepsilon_{p(k)}$ and $P_m\varepsilon_m$ are equal to the average number of ultra-violet photons and metastables, respectively, which are normalized by the number of electrons in an avalanche, i.e., the gas gain G. The gas gain strongly depends on the anode voltage V_a, as described in Section 3. Other parameters in Eqs. (7), (9) and (10) are approximately independent of the voltage.

The electric discharge takes place when R defined by Eq. (6) becomes more than unity,

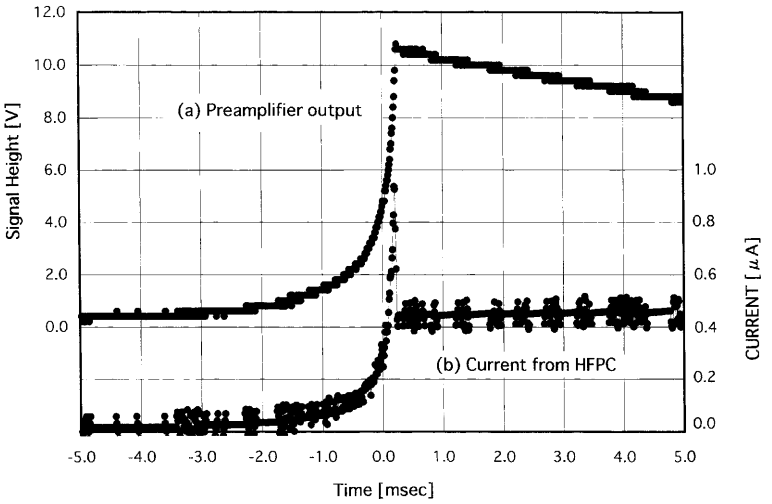

Fig. 4. Self-sustained electric discharge, which limits the counter operation of HFPC in proportional region: (a) preamplifier output; (b) discharge current estimated with the transfer function of the preamplifier.

$$R \geqslant 1. \tag{11}$$

The HFPC operation in the proportional region is practically limited by the electric discharge as shown in Fig. 4; the pressure of the filled helium is 10.6 Torr at 4.2 K and the anode voltage is a little higher than 1250 V. The voltage signal of the electric discharge observed with a charge-sensitive preamplifier is given by Fig. 4(a), while the output current from HFPC, which was deduced from the voltage signal using the transfer function of the preamplifier, is given by Fig. 4(b). In the electric discharge, the current exponentially increases and suddenly falls down to the level of about half at the peak current. Detailed discussion on the structure of the discharge current was given in the previous work [9].

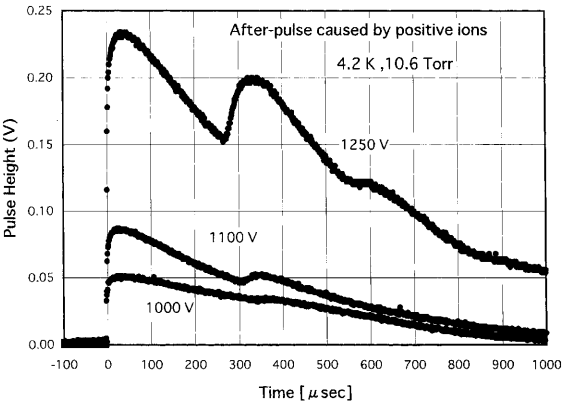

Fig. 5. After-pulses appearing in output signals from the HFPC: these pulses result from the secondary electron emission caused by the collision of positive helium ion clusters with cathode materials.

4.2. After-pulse caused by positive ions

In Fig. 5, pulse shapes of the preamplifier outputs observed at $V_a = 1000$, 1100 and 1250 V are shown; the pressure of the filled helium is 10.6 Torr at 4.2 K. After-pulses clearly appear as humps on the pulses at $V_a = 1100$ and 1250 V. These pulses are caused by new avalanches, which are induced by electrons emitted by the collision of positive helium ions with cathode. The new avalanches result in the first after-pulse, while avalanches by the primary electrons result in the main pulse. Successive after-pulses are produced with the same mechanism as for the first after-pulse; the second after-pulse is seen in the pulse shapes at $V_a = 1250$ V. The time interval between the main pulse and the after-pulse is a sum of the drift time of positive helium ions from anode to cathode and that of electrons from cathode to anode. Since the drift time of helium ions (250–400 μs) is much

slower than that of electrons (1–2 μs), the time delay of the after pulse mainly comes from the drift of the helium ion. As V_a is increased, the hump is larger and the time interval is shorter, as expected.

A ratio of the area of the first hump to that of the main pulse is equal to R_i given by Eq. (7). The R_i value obtained with the pulse at $V_a = 1250$ V is 0.38, with which Γ_i $(= R_i/G)$ is estimated to 2.5×10^{-3}. This value agrees with the previous measurement at a little higher temperature, i.e., ~5 K [8].

4.3. Formation of helium ion clusters at low temperatures

The Γ_i value experimentally determined is two orders in magnitude smaller than that at room temperature, e.g., 0.13 for the collision of He_2^+ with molybdenum [16,17]. The formation of positive helium ion clusters with large sizes is responsible for the favorable decrease of Γ_i in the HFPC operation at low temperatures.

In pure helium gas, helium ions He^+ is changed to molecular ions He_2^+ through the three-body collision,

$$He^+ + 2He \rightarrow He_2^+ + He. \quad (12)$$

Its reaction rate is $\sim 85p^2$ s^{-1} at room temperature [18]. The molecular ions He_2^+ are produced also through the Hornbeck–Molnar process (1) at room temperature, as discussed in Section 3.

These He_2^+ ions are moderated in thermal energies by colliding repeatedly with helium atoms in the drift from anode to cathode. Then, through successive reactions of

$$He_n^+ + 2He \rightarrow He_{n+1}^+ + He \quad (n = 1, 2, \ldots), \quad (13)$$

the molecular ion with larger size n grows up [19]. Molecular helium ions with a size up to 4 were observed at low temperatures down to liquid-nitrogen temperature [20,21]. The size at lower temperatures near 4.2 K may be more than 10; further discussion on the helium ion cluster was given in our previous work [8].

4.4. After-pulse caused by photons

In Fig. 6, rise parts of preamplifier outputs observed at $V_a = 1000$, 1100, 1200 and 1250 V are shown; the pressure of the filled helium is 10.6 Torr at 4.2 K. As seen in Fig. 6, there is a faint slope on the output at $V_a = 1250$ V, which appears about 2 μs later after their start time. This is the after-pulse caused by the electrons, which are emitted by the photo-effect of ultra-violet photons at cathode. The photons produced in electron avalanches travel to cathode in a very short time and then emit electrons from cathode through the photo-effect. Therefore, new avalanches with a time delay of 1–2 μs, which correspond to the drift time of the electrons from cathode to anode, are superimposed on the avalanches initiated by the primary ionization. As similar to R_i, the parameter R_p is given by a ratio of the area of the faint bump to that of the main pulse. The R_p value obtained with the pulse at $V_a = 1250$ V in Fig. 6 is about 4×10^{-2}.

4.5. Radiative transition of excited helium atoms

Ultra-violet photons produced in electron avalanches partially come from radiative transitions of excited helium atoms He^*. Resonance photons are emitted by the transition of He^* $(n^1P; n \geqslant 2)$ to

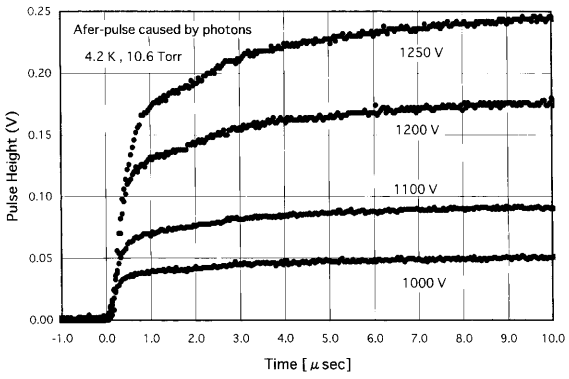

Fig. 6. Rise parts of output signals from HFPC, in which after-pulses are included as faint bumps: these pulses result from the secondary electron emission caused by the photo-effect of photons from the radiative transitions of highly-excited helium atoms.

the ground, He(1^1S); their energies are higher than 20 eV. These photons are resonantly absorbed by helium gas atoms, which re-emit photons with the same energy or de-excited to He^* in lower states through the collision with helium gas atoms [22,23]. Thus, the resonance radiations are imprisoned and disappear through the collisional de-excitations before arriving at cathode in the HFPC with an ordinary size.

Non-resonance photons are emitted through the radiative transitions of the excited atoms to He^*(2P) or He^m(2S), i.e., $n^1S\ (n \geqslant 3) \rightarrow 2^1P^0$, $n^1D\ (n \geqslant 3) \rightarrow 2^1P^0$, $n^1P^0\ (n \geqslant 2) \rightarrow 2^1S$, $n^3S\ (n \geqslant 3) \rightarrow 2^3P^0$, $n^3D\ (n \geqslant 3) \rightarrow 2^3P^0$ and $n^3P^0\ (n \geqslant 2) \rightarrow 2^3S$. Their energies are 5 eV at the highest and their transition probabilities are the order of 10^6–10^7 s^{-1}, as listed in Table 3. Since pure helium gas is transparent to these non-resonance photons, the photons collide with cathode materials.

Since the work function of most of metals is in the range of 3–5 eV, photons with energies higher than about 3 eV can contribute the electron emission from cathode. Excited helium with $n \geqslant 4$ states emit photons with such energies, of which the population $P_{p(1)}$ in Eq. (9) is at most 0.2 ($= 8.4/40.5$) per an ionization event in the electron avalanche, as seen in Table 2, where the subscript p(1) corresponds to the photons with low energies of 3–5 eV. The coefficient $\Gamma_{p(1)}$ is the order of 0.01 [26].

The parameter $\varepsilon_{p(1)}$ in Eq. (9) is approximately given by

$$\varepsilon_{p(1)} = \lambda/(\lambda + D_{hm} + D_{cd} + D_{ot}). \quad (14)$$

In the above equation, the probability of the radiative transitions, λ, is the order of 10^7 s^{-1} as seen in Table 3, while the rate of the Hornbeck–Molnar process D_{hm} and that of the collisional de-excitation D_{cd} are the order of 10^{10} s^{-1} at the normal condition. The rate of other competing processes D_{ot} is assumed to be much smaller than D_{hm} and D_{cd}. Thus, $\varepsilon_{p(1)}$ is the order of 10^{-3} at room temperature. According to Eq. (9), $R_{p(1)}$ is very roughly estimated to 4×10^{-4} for $G = 200$, which is two orders in magnitude smaller than the present experimental value obtained at 4.2 K, i.e., 4×10^{-2}.

The enhancement of radiative transition comes from the suppression of the collisional de-excitations of excited helium atom at low temperatures near 4.2 K. This is quite similar to the case of Hornbeck–Molnar process, as discussed in Section 3.

Table 3
Radiative transitions of excited states

Transition	Photon energy (eV)	Probability (10^8 s^{-1})
$2^3P \rightarrow 2^3S$	1.145	0.1022
$2^1P \rightarrow 2^1S$	0.602	0.0190
$2^1P \rightarrow 1^1S$	21.230	17.9900
$3^3S \rightarrow 2^3P$	1.755	0.2786
$3^1S \rightarrow 2^1P$	1.703	0.1829
$3^3P \rightarrow 2^3S$	3.189	0.0948
$3^1P \rightarrow 2^1S$	2.472	0.1338
$3^1P \rightarrow 1^1S$	23.090	5.6600
$3^3D \rightarrow 2^3P$	2.110	0.7053
$3^1D \rightarrow 2^1P$	1.856	0.6339

4.6. Role of metastable helium atoms

At $V_a = 1250$ V for the present HFPC, which is a little lower than the voltage to induce the electric discharge, we have obtained $R_i = 0.38$ and $R_{p(1)} = 0.04$, as explained before. The sum of R_i and $R_{P(1)}$, i.e., 0.42, is much smaller than unity. According to the relation (11), this fact indicates that, except the positive helium ion cluster, He_n^+, and the non-resonance photons emitted from highly-excited helium atoms, He^* ($n \geqslant 4$), there exist other active particles which emit secondary electrons through the collision with cathode.

A lot of metastable atoms He^m(2S) are produced through the direct excitation of helium gas by electrons and the de-excitation of excited helium atoms in electron avalanches. The intrinsic life time is 20 ms for the singlet, $He^m(2^1S)$, and 6×10^5 s for the triplet, $He^m(2^3S)$ [25]. In spite of the long life times, they cannot arrive at cathode in the HFPC because most of them are de-excited through collisions with helium gas atoms in the diffusion. In the operation of HFPC, these metastables $He^m(2^1S)$ and $He^m(2^3S)$ play a role to produce other active particles, as discussed below.

Another origin of the active particles may be the product by the collision of $He^*(2^1P)$ with helium gas atoms. One of the decaying paths of $He^*(2^1P)$ is the formation of the radiating molecules, $He_2^*(D^1\Sigma_g^+)$, which is produced through three-body collisions of $He^*(2^1P)$ with helium gas atoms and then emits photons with an energy of 13.1–19.4 eV as a result of the successive decomposition [26]. However, this process is unlikely at room or lower temperatures because the $D^1\Sigma_g^+$ state has a 0.63-eV potential hump, which is much higher than the thermal energy (0.026 eV at room temperature) [27,28].

4.7. Creation of excited molecules, $He_2^*(A^1\Sigma_u^+)$ and $He_2^m(a^3\Sigma_u^+)$

The de-excitation process of the singlet $He^m(2^1S)$ is different from that of triplet $He^m(2^3S)$. The radiative molecule, $He_2^*(A^1\Sigma_u^+)$, is produced through two-body or three-body collisions of $He^m(2^1S)$ with helium atoms,

$$He^m(2^1S) + He \rightarrow He_2^*(A^1\Sigma_u^+), \tag{15}$$

$$He^m(2^1S) + 2He \rightarrow He_2^*(A^1\Sigma_u^+) + He, \tag{16}$$

where the reaction rate is $\sim 220p\ s^{-1}$ for the process (15) and $\sim 1.4p^2\ s^{-1}$ for the process (16) [29]. At the normal condition, the rate equals to $1.7 \times 10^5\ s^{-1}$ for the process (15) and $8.1 \times 10^5\ s^{-1}$ for the process (16). In the process (15), $He_2^*(A^1\Sigma_u^+)$ successively decomposes to two helium atoms, radiating photons with an energy of 20.5–20.6 eV. The molecule $He_2^*(A^1\Sigma_u^+)$ produced in the process (16) de-excites to $He_2(X^1\Sigma_g^+)$, radiating photons with an energy of 11.2–20.6 eV. These photons from the de-excitation of $He_2^*(A^1\Sigma_u^+)$ are not absorbed in helium gas atoms. Most of them travel to cathode, where secondary electrons are emitted by the photo-ionization with cathode materials. The second component of the non-resonance radiations, i.e., $R_{p(2)}$ in Eq. (8), comes from $He_2^*(A^1\Sigma_u^+)$. The radiative transition of $He^m(2^1S)$ can be neglected because of its small transition probability, i.e., $\sim 50\ s^{-1}$.

The metastable molecule, $He_2^m(a^3\Sigma_u^+)$, is produced through the three-body collision of $He^m(2^3S)$ with helium gas atoms [30],

$$He^m\ (2^3S) + 2He \rightarrow He_2^m(a^3\Sigma_u^+) + He. \tag{17}$$

Its rate is $0.2p^2\ s^{-1}$ which corresponds to $1.5 \times 10^5\ s^{-1}$ at the normal condition. The intrinsic lifetime of $He_2^m(a^3\Sigma_u^+)$ is longer than 50 ms [31]. A part of $He_2^m(a^3\Sigma_u^+)$ can arrive at cathode by diffusion where secondary electrons are emitted. Therefore, the parameter R_m given by Eq. (10) is attributed to the metastable molecule $He_2^m(a^3\Sigma_u^+)$.

As similar to the cases of Hornbeck–Molnar process and collisional de-excitation of excited helium, the atom–atom collision processes (15)–(17) may be suppressed at the low temperatures near 4.2 K. Then, the reaction rates of those processes are expected to be the order of 10^4–$10^5\ s^{-1}$ at the low temperatures; the rates are at most the order of $10^6\ s^{-1}$ at the normal condition. Therefore, the photons from $He_2^*(A^1\Sigma_u^+)$ are spread in the time interval of the order of 10–100 μs, which is too long to observe the photons as after-pulse. This is a reason why we could not observe the after-pulses caused by the non-resonance photons from the molecule, $He_2^*(A^1\Sigma_u^+)$. Because there is a time delay of the order of several ms between the creation of $He_2^m(a^3\Sigma_u^+)$ and its arrival at cathode by diffusion, it is also very difficult to observe directly the secondary electron emission caused by $He_2^m(a^3\Sigma_u^+)$.

5. A simple model for the HFPC operation

A simplified model for the operation of HFPC is given by Fig. 7, which illustratively shows the roles of excited helium atoms and molecules, positive ions and ultra-violet photons, on the electron avalanche and the secondary electron emission from cathode. Each process to produce those active particles is listed in Table 4; the notations R1, R2 and others in Fig. 7 correspond to the same notations to indicate each reaction in the table.

In the present model, two collision processes contribute to the electron avalanches, i.e.,

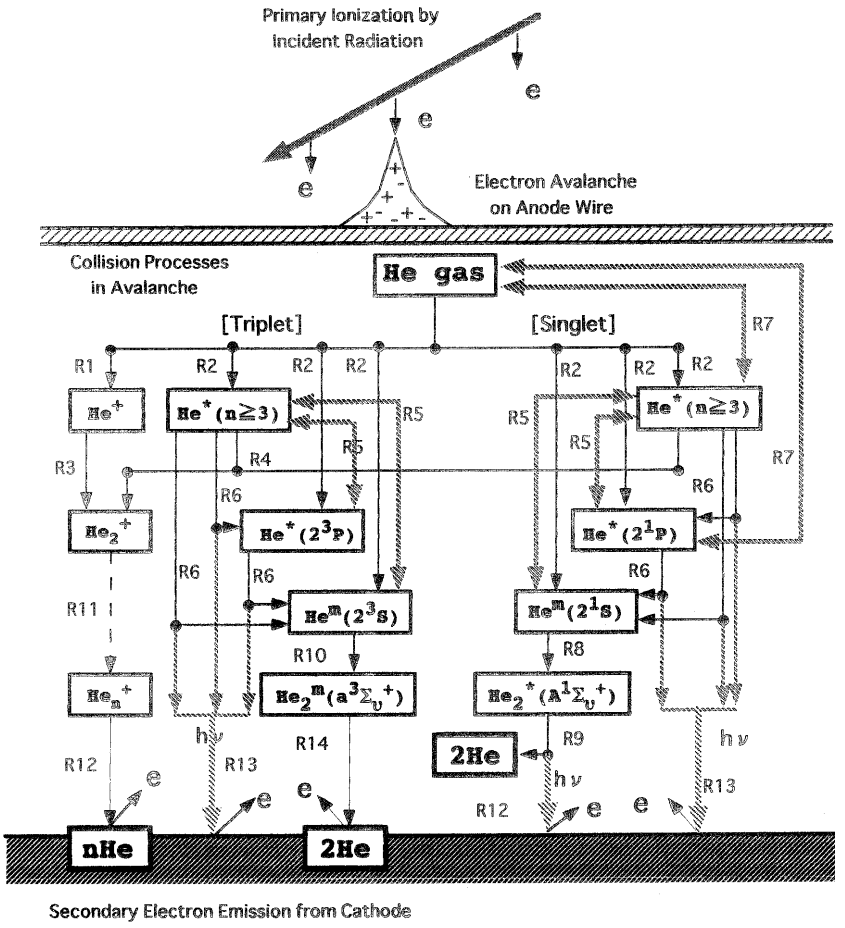

Fig. 7. A simplified picture of the operation of the helium-filled proportional counter at low temperatures near 4.2 K: the numbers, i.e., R1, R2,..., R12, correspond to atomic processes listed in Table 4.

1. R1 in Fig. 7 and Table 1: ionization of helium atoms by electron impact and
2. R4: collisional ionization of He^* ($n \geqslant 3$), i.e., Hornbeck–Molnar process.

There are four kinds of active particles, which originate the secondary electron emission from cathode, i.e.,

1. R12: positive helium ion clusters,
2. R6: photons from the radiative transition of He^* ($n \geqslant 4$),
3. R9: photons from the radiative decay of $He_2^*(A^1\Sigma_u)$ and
4. R14: metastable $He_2^m(a^3\Sigma_u)$.

The operation of HFPC is determined by eleven parameters, which are related to the production of the active particles, i.e., G and Γ_i in Eq. (7), $\Gamma_{p(1)}$, $\Gamma_{p(2)}$, $P_{p(1)}$, $P_{p(2)}$, $\varepsilon_{p(1)}$ and $\varepsilon_{p(2)}$ in Eqs. (8) and (9) and Γ_m, P_m and ε_m in Eq. (10).

As shown in the present work, it is possible to determine experimentally G from the gas gain curve, and Γ_i and $\Gamma_{p(1)}$ from the after-pulses at 4.2 K. The parameters $P_{p(1)}$ and $\varepsilon_{p(1)}$ have been estimated according to the discussion in Section 4. A very rough estimation has been performed for other parameters, i.e., $\Gamma_{p(2)}$, $P_{p(2)}$ and $\varepsilon_{p(2)}$ for the photons from $He_2^*(A^1\Sigma_u^+)$ and Γ_m, P_m and ε_m for the metastables $He_2^m(a^3\Sigma_u^+)$. The probable values for the 11 parameters of the present HFPC at 4.2 K are listed in Table 5; only the upper limits for $\varepsilon_{p(2)}$ and ε_m have been obtained because of no data

Table 4
Atomic and molecular processes related to the HFPC operation

Number[a]	Reactions	n[b] or E_p[c]	Reference
R1	Ionization by electron	–	–
R2	Excitation by electron	–	–
R3	$He^+ + 2He \rightarrow He_2^+ + He$	$n = 85p^2, 4.9 \times 10^7$	[18]
R4	$He^* + He \rightarrow He_2^+ + e$	$n = 10^7 p$ $(n \geqslant 3)$	[10,11]
R5	Collisional relaxations	–	[12]
R6	Radiative transition	–	–
R7	Imprisonment of resonance photons	–	[22,23]
R8	He^m $(2^1S) + He \rightarrow He_2^*(A^1\Sigma_u^+)$	$n = 220p, 1.7 \times 10^5$	[29]
	He^m $(2^1S) + 2He \rightarrow He_2^*(A^1\Sigma_u^+) + He$	$n = 1.4p^2, 8.1 \times 10^5$	[29]
R9	$He_2^*(A^1\Sigma_u^+) \rightarrow 2He + h\nu$	$E_p = 20.5$–20.6 eV	[29]
	$He_2^*(A^1\Sigma_u^+) \rightarrow He(X^1\Sigma_g^+) + h\nu$	$E_p = 11.2$–20.6 eV	[30]
R10	He^m $(2^3S) + 2He \rightarrow He_2^m(a^3\Sigma_u^+) + He$	$n = 0.2p^2, 1.5 \times 10^5$	[30]
R11	$He_{n-1}^+ + 2He \rightarrow He_n^+ + He$	–	[19]
R12	$He_n^+ + M \rightarrow nHe + M^+ + e$	–	–
R13	$h\nu + M \rightarrow M^+ + e$	–	[24]
R14	$He_m^2(a^3\Sigma_u^+) + M \rightarrow M^+ + e$	–	–

[a] The number in this column corresponds to that of reaction number in text and Fig. 7.
[b] Reaction rate ($1\ s^{-1}$) as the function of pressure (Torr) and that at the normal condition.
[c] Energy of ultra-violet photon.

Table 5
Probable values of parameters in the present model for the HFPC operation[a]

Parameters	Probable values	
	4.2 K	Room temperature
G_{max}	200[b]	7.7[c]
$R_i[\equiv G\Gamma_i]$	0.38[b]	1.0
Γ_i	2.5×10^{-3}[b]	0.13
$R_{p(1)}[\equiv GP_{p(1)}\varepsilon_{p(1)}\Gamma_{p(1)}]$	0.04[b]	1.5×10^{-5}
$P_{p(1)}$	0.2	0.2
$\varepsilon_{p(1)}$	0.1	1×10^{-3}
$\Gamma_{p(1)}$	0.01	0.01
$R_{p(2)}[\equiv GP_{p(2)}\varepsilon_{p(2)}\Gamma_{p(2)}]$	<0.58[d]	<0.022
$P_{p(2)}$	>0.1	>0.1
$\varepsilon_{p(2)}$	<0.29	<0.29
$\Gamma_{p(2)}$	0.1	0.1
$R_m[\equiv GP_m\varepsilon_m\Gamma_m]$	<0.58[e]	<0.022
P_m	>0.2	>0.2
ε_m	<1.0	<1.0
Γ_m	0.01	0.01

[a] Helium gas is filled at the normal condition.
[b] Experimentally determined at the anode voltage of 1250 V; other values are estimated from related data.
[c] The anode voltage to obtain this gain is 600 V.
[d] Assumed to be $R_{p(2)} = 0$.
[e] Assumed to be $R_m = 0$.

on the other collisional de-excitation processes for $He_2^*(A^1\Sigma_u^+)$ and $He_2^m(a^3\Sigma_u^+)$.

As seen in Table 5, the large changes in Γ_i and $\varepsilon_{p(1)}$ take place when the HFPC is cooled down from room temperature to 4.2 K. The parameter Γ_i is decreased by the order of two because of the formation of helium ion clusters. The parameter $\varepsilon_{p(1)}$ is enhanced by the order of two because of the suppression of the atom–atom collision of He^* $(n \geqslant 4)$. The drastic decrease in Γ_i results in the relatively high gas gain, i.e., $G = 200$, at the low temperatures. The available gas gain at room temperature is at most 10 because of the large value of Γ_i, i.e., 0.13.

6. Concluding remarks

In the present work, we have not been able to separate the contributions of $He_2^*(A^1\Sigma_u^+)$ and $He_2^m(a^3\Sigma_u^+)$ to the secondary electron emission from cathode. It is expected that the photons from the decay of $He_2^*(A^1\Sigma_u^+)$ considerably distort the pulse shape of output signals from the preamplifier. As shown in our previous work [9], there are two exponential components in the shape of

observed current signal of electric discharge. This probably indicates that the electrons emitted by the collision of $He_2^m(a^3\Sigma_u^+)$ with cathode, which have a time delay of the order of several ms, contribute to the second component with a larger exponential coefficient. Thus, it may be possible to determine the parameters $R_{p(2)}$ and R_m with careful analyses for the pulse shape of output signals and the shape of discharge current, respectively. New measurement to determine $R_{p(2)}$ and R_m is now in progress.

According to the present model, Γ_i further decreases when number density of helium gas is higher or temperature is lower. Then, since the electron emission caused by the ion clusters at cathode is more suppressed, the emission caused by the photons from $He_2^*(A^1\Sigma_u^+)$ and the metastables $He_2^m(a^3\Sigma_u^+)$ becomes dominant in the electric discharge. On the contrary, the electron emission by the ion clusters becomes dominant in the electric discharge when the density is lower or the temperature is higher. It has been found by our preliminary measurement [32], that the maximum available gas gain G_{max} becomes higher as the density is increased up to three times of the density at the normal condition. We already found that G_{max} becomes lower when the gas temperature is cooled down from 4.2 to 1.75 K [3].

Further studies in different conditions of the number density and the temperature are clearly necessary to elaborate the present model. In principle, the number density can be increased to about 70 times of that at the normal condition. It is very interesting to observe the HFPC operation at such high densities, which show more clearly the role of $He_2^*(A^1\Sigma_u^+)$ and $He_2^m(a^3\Sigma_u^+)$ in the electric discharge.

References

[1] S. Kishimoto, Y. Isozumi, R. Katano, H. Takekoshi, Nucl. Instr. and Meth. A 262 (1987) 413.
[2] Y. Isozumi, S. Kishimoto, R. Katano, H. Takekoshi, Rev. Sci. Instr. 58 (1987) 293.
[3] Y. Isozumi, S. Ito, T. Fujii, R. Katano, Rev. Sci. Instr. 60 (1989) 3262.
[4] T. Kobayashi, K. Fukumura, Y. Isozumi, R. Katano, Hyp. Int. 57 (1990).
[5] T. Fujii, M. Takano, R. Katano, Y. Bando, Y. Isozumi, J. Appl. Phys. 68 (1990) 1735.
[6] Y. Isozumi, T. Fujii, Other applications of HFPC to REMS are reviewed, Current Topics in Crystal Growth Res. 1, Research Trends, India, 1994, p. 187.
[7] S. Kishimoto, Y. Isozumi, Nucl. Instr. and Meth. A 286 (1990) 262.
[8] Y. Isozumi, R. Katano, S. Ito, S. Kishimoto, Nucl. Instr. and Meth. A 355 (1995) 443.
[9] S. Masaoka, R. Katano, Y. Isozumi, Nucl. Instr. and Meth. B 160 (2000) 172.
[10] J.A. Hornbeck, J.P. Molnar, Phys. Rev. 84 (1969) 621.
[11] H.F. Wellenstein, W.W. Robertson, J. Chem. Phys. 56 (1972) 1077.
[12] H.F. Wellenstein, W.W. Robertson, J. Chem. Phys. 56 (1972) 1072.
[13] G.D. Alkhazov, A.A. Vorob'ev, Phys. Lett. 29A (1969) 25.
[14] A. von Engel, Ionized Gas, Clarendon Press, Oxford, 1965.
[15] L.M. Chanin, G.D. Rork, Phys. Rev. 133 (1964) 1005.
[16] H.D. Hagstrum, Phys. Rev. 89 (1953) 244.
[17] H.D. Hagstrum, Phys. Rev. 96 (1954) 325.
[18] D. Smith, M.J. Copsey, J. Phys. B 1 (1968) 650.
[19] N. Kobayashi, T. Kojima, Kaneko, J. Phys. Soc. Jpn. 57 (1988) 1528.
[20] F.W. Lee, C.B. Collins, R.A. Waller, J. Chem. Phys. 65 (1976) 1605.
[21] P.L. Patterson, J. Chem. Phys. 48 (1968) 3625.
[22] T. Holstein, Phys. Rev. 72 (1947) 1212.
[23] T. Holstein, Phys. Rev. 83 (1951) 1159.
[24] R.F. Stebbings, Proc. Roy. Soc. A 241 (1957) 270.
[25] G. Bekefi, Principle of Laser Plasmas, Wiley, New York, p. 212.
[26] M.G. Payne, C.E. Klots, G.S. Hurst, J. Chem. Phys. 63 (1975) 1422.
[27] M. Gand, A. Bouchoule, J. Stevefelt, Appl. Phys. Lett. 35 (1979) 50.
[28] S.L. Guberman, W.A. Goddard III, Phys. Rev. A 12 (1975) 1203.
[29] M.G. Payne, G.S. Hurst, M.H. Nayfeh, J.P. Judish, C.H. Chen, E.B. Wagner, J.P. Young, Phys. Rev. Lett 35 (1975) 1154.
[30] G. Myers, A.J. Cunningham, J. Chem. Phys. 67 (1977) 247.
[31] A.V. Phelps, Phys. Rev. 99 (1955) 1307.
[32] S. Masaoka, R. Katano, Y. Isozumi, to be published.